Structure-Directing Effects in Zeolite Synthesis: A Single-Crystal X-ray Diffraction, ^{29}Si MAS NMR, and Computational Study of the Competitive Formation of Siliceous Ferrierite and Dodecasil-3C (ZSM-39)

Scott J. Weigel, Jean-Christophe Gabriel, E. Guttierez Puebla, A. Monge Bravo, Neil J. Henson, Lucy M. Bull, and Anthony K. Cheetham*

Contribution from the Materials Research Laboratory, University of California, Santa Barbara, California 93106

Received July 21, 1995[⊗]

Abstract: The competitive formation of the zeolites ferrierite and dodecasil-3C has been studied under a variety of synthetic conditions involving HF/pyridine as a solvent together with other amines. Single crystal X-ray diffraction measurements on the siliceous zeolite ferrierite product ($Si_{18}O_{36}$·$1.9C_5H_5N$·$0.1C_3H_9N$, space group *Pmnn*, $a = 18.8273(6)$ Å, $b = 14.095(1)$ Å, $c = 7.4318(7)$ Å, $V = 1972.2(3)$ Å^3, $Z = 2$, $R = 3.1\%$) reveal that it contains pyridine in both channels. Small amounts of propylamine are found in the main channel. The dodecasil-3C, by contrast, contains pyridine in the larger cavities and propylamine in the smaller ones ($Si_{17}O_{34}$·$0.8C_5H_5N$·$0.25C_3H_9N$, space group *I42d*, $a = 13.639(2)$ Å, $c = 19.512(4)$ Å, $V = 3629.67(6)$ Å^3, $Z = 4$, $R = 6.8\%$). Both the synthetic observations and our computer simulations indicate that the dodecasil-3C is thermodynamically more stable than the ferrierite product, which forms under kinetic control at lower temperatures or shorter reaction times. An additional phase, identified as a propylammonium hexafluorosilicate, is also present during the course of the reaction. The propylammonium cation appears to play a dual role: acting as a pH buffer and nucleating the ferrierite phase. The dodecasil-3C phase is probably nucleated by pyridinium ions.

Introduction

The role of organic templates or structure-directing agents in zeolite synthesis has been widely discussed in the literature, but no general principles have yet emerged and there is ample evidence to indicate that the role of these organic additives is quite varied.[1,2] In hexagonal faujasite (EMT), for example, the crown ether template (18-crown-6) appears to be laid down in pockets on the growing surface, where the spatial fit is very good, and the structure builds up along [001], one layer at a time; the additional use of 15-crown-5 leads to the formation of cubic stacking faults.[3] Similarly, in ZSM-5 there is a clear relationship between the shape of the template cation (typically tetrapropylammonium, TPA) and the architecture of the pore system.[4] There is also evidence in this system for the existence of preorganized inorganic−organic composite structures during early stages of the reaction.[5] In other systems, however, there is no such relationship and additional factors such as the influence of the organic phase on the gel chemistry are considered to be important.[6] The synthesis of siliceous ferrierite, which can be carried out in a HF/pyridine solvent system in the presence of propylamine and excess pyridine,[7] affords an interesting opportunity to explore the role of the templating molecules; the reaction yields crystals that are sufficiently large for X-ray crystallographic studies, and by slightly altering the synthetic conditions dodecasil-3C (ZSM-39, MTN) can be obtained as the preferred product. Furthermore, the system permits us to examine the role of HF in the synthesis of these particular zeolites; fluoride species are now used widely in reactions of this type and the nature of their role has been discussed.[8]

The zeolite ferrierite (FER) is well-known both in nature and as a synthetic material.[9] Its commercial utility has been restricted by its tendency to contain stacking faults,[10,11] but interest in its structure and properties has recently been stimulated by reports that it is the preferred catalyst for deNOx reactions with methane as the reductant[12] and an excellent, shape-selective catalyst for the isomerization of *n*-butenes to isobutene.[13] The latter is an important feedstock for the production of methyl *tert*-butyl ether (MTBE), which is a commercial oxygenate additive in unleaded motor fuel. Ferrierite is typically synthesized as an aluminosilicate with Na,K counterions, but it can be prepared in its siliceous form by both aqueous[14] and non-aqueous routes,[7] and the structure of the

[⊗] Abstract published in *Advance ACS Abstracts,* February 1, 1996.

(1) Davis, M. E.; Lobo, R. F. *Chem. Mater.* **1992**, *4*, 756.
(2) Lok, B. M.; Cannan, T. R.; Messina, C. A. *Zeolites* **1983**, *3*, 282.
(3) Terasaki, O.; Ohsuna, T.; Alfredsson, V.; Bovin, J.-O.; Watanabe, D.; Carr, S. W.; Anderson, M. W. *Chem. Mater.* **1993**, *5*, 452.
(4) Price, G. D.; Pluth, J. J.; Smith, J. V.; Bennett, J. M.; Patton, R. L. *J. Am. Chem. Soc.* **1982**, *104*, 5971.
(5) Burkett, S. L.; Davis, M. E. *J. Phys. Chem.* **1994**, *98*, 4647.
(6) Zones, S. I.; Santilli, D. S. In *Proceedings from the 9th International Zeolite Conference*; von Ballmoos, R., Higgins, J. B., Treacy, M. M. J., Eds.; Butterworth-Heinemann: Boston, 1992; p 171.
(7) Kuperman, A.; Nadimi, S.; Oliver, S.; Ozin, G. A.; Garces, J. M.; Olken, M. M. *Nature* **1993**, *365*, 239.
(8) Kessler, H.; Patarin, J.; Schott-Darie, C. In Studies in Surface Science and Catalysis. *Advanced Zeolite Science and Applications*; Jansen, J. C., Stöcker, M., Karge, H. G.; Weitkamp, J., Eds.; Elsevier: Amsterdam, 1994; p 75.
(9) Wise, W. S.; Tschernich, R. W. *Am. Mineral.* **1976**, *61*, 60.
(10) Gramlich-Meier, R.; Meier, W. M.; Smith, B. K. *Z. Kristallogr.* **1984**, *169*, 201.
(11) Rice, S. B.; Treacy, M. M. J.; Newsam, J. M. *Zeolites* **1994**, *14*, 33.
(12) Armour, J. Private communication.
(13) Mooiweer, H. H.; deJong, K. P.; Kraushaar-Czarnetzki, B.; Stork, W. H. J.; Krutzen, B. C. H. In *Studies in Surface Science and Catalysis*; 1994, Vol. 84C, p 2327.
(14) Gies, H.; Gunawardane, R. P. *Zeolites* **1987**, *7*, 442.
(15) Morris, R. E.; Weigel, S. J.; Henson, N. J.; Bull, L. M.; Janicke, M. T.; Chmelka, B. F.; Cheetham, A. K. *J. Am. Chem. Soc.* **1994**, *116*, 11854.

0002-7863/96/1518-2427$12.00/0

siliceous material, with the templates removed, has been studied by synchrotron X-ray and neutron powder diffraction.[15]

The crystal structure of ferrierite (FER) was first solved by Vaughan[16] on a magnesium-containing mineral sample from Kamloops Lake, Canada, and the essential features have been confirmed by a number of other workers.[17,18] It is a member of the pentasil family of zeolites, which includes mordenite and ZSM-5, and is based on 5-ring building units, stacked in the [001] direction. These are connected to form oval 10-ring channels running parallel to [001], which are intersected by 8-ring channels running parallel to [010] (Figure 1). Also present in the structure is a small cage, bounded by 6-rings, centered at 0,0,0. The space group has been the subject of some discussion and has been variously reported to be *Immm*, *Pmnn*, or $P2_1/n$.[14−17] The orthorhombic description in *Pmnn* was chosen for the present work.

The structure of the clathrasil, dodecasil-3C (MTN), comprises two types of cage, one a smaller pentagonal dodecahedron and the other a larger hexadecahedron, which are fused through 5-ring windows (Figure 2). The room temperature crystal structure of MTN synthesized in the presence of HF/pyridine, but in the absence of propylamine, reveals that pyridine is entrapped in the larger cage.[19] At higher temperatures, there is a phase transition to a cubic phase.[20]

Experimental Section

1. Synthesis and Thermogravimetric Analysis. The hydrothermal crystallization of the siliceous ferrierite was carried out in Teflon-lined 23- and 45-mL Parr digestion bombs according to the method of Kuperman *et al.*[7] The reactants used were pyridine [Pyr] (Fisher), propylamine [$PrNH_2$] (Aldrich), HF/pyridine [HF/Pyr] (70 wt % HF, Aldrich), Cab-O-Sil (Kodak M-5, scintillation grade), and deionized H_2O. A typical reaction contained these components in the following molar ratios: $1.5SiO_2$:2HF/pyr:$8H_2O$:$4PrNH_2$:16pyr. The appropriate amounts of water, propylamine, pyridine, and HF/pyridine were added together first in the Teflon liner and the clear solution was stirred for 15 min. While stirring the amine solution, the silica was added in 0.1-g quantities. The mixture was then stirred for an hour to ensure that all the silica was dissolved. The resulting solution was clear and had a pH of 10. The autoclaves were heated to 170 °C in a forced draft oven with temperature control within 1 °C and left for 5−7 days to crystallize. After the hydrothermal treatment, the autoclave was removed from the oven and quenched in cold water. The resulting zeolite was separated from its mother liquor by vacuum filtration, washed in deionized water, rinsed with acetone, and dried at room temperature.

Variations on the above procedure were explored, as set out in Table 1. In particular, the effects of varying the temperature and duration of the reaction, varying the HF/Pyr concentration, and replacing the propylamine by other amines were examined. In a number of instances, alternative products, especially dodecasil-3C, were obtained.

Thermal analysis of the templated ferrierite was performed on a Netzsch combined TGA/DTA STA 409 system equipped with a 100 cm^3/min O_2 flow. Using a 10 °C/min ramp rate from 25 to 1100 °C four distinct weight losses are observed. The low-temperature weight losses between 30 and 417 °C (4.7%) arise from the desorption of the weakly bound propylamine and pyridine in the 10-ring channel, and the final weight change between 552 and 850 °C (6.0%) corresponds quantitatively to the loss of pyridine from the more tightly bound side channel. The DTA shows that there is an endotherm at 223 °C, and three exotherms at 332, 530, and 657 °C.

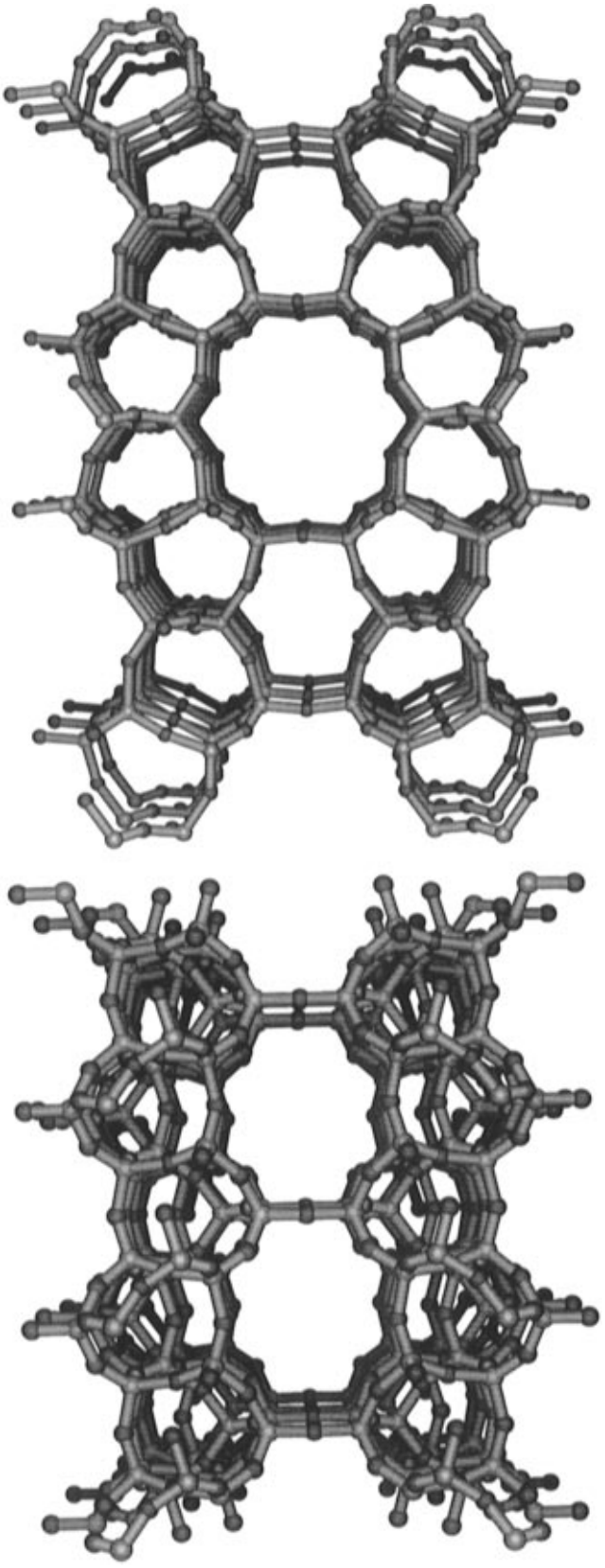

Figure 1. The structure of ferrierite (*Pmnn* symmetry) viewed (a, top) down the [001] direction showing the 10-ring channels and (b, bottom) down the [010] showing the 8-ring channel.

2. Single-Crystal X-ray Diffraction. A colorless plate-like crystal of the ferrierite reaction product, size 250 μm × 250 μm × 10 μm, was mounted on a CAD-4 MACH diffractometer, equipped with a Rigaku rotating anode source (graphite-monochromated Cu Kα radia-

(16) Vaughan, P. A. *Acta Crystallogr.* **1966**, *21*, 983.
(17) Alberti, A.; Sabelli, C. *Z. Kristallogr.* **1987**, *178*, 249.
(18) Gramlich-Meier, R.; Gramlich, V.; Meier, W. M. *Am. Mineral.* **1985**, *70*, 619.
(19) Chae, H. K.; Klemperer, W. G.; Payne, D. A.; Suchicital, C. T. A.; Wake, D. R.; Wilson, S. R. In *Materials for Nonlinear Optics*; ACS Symposium Series No. 455; Marder, S. R., Sohn, J. E., Stucky, G. D., Eds.; American Chemical Society: Washington, DC, 1991; p 528.
(20) Strobl, H.; Fyfe, C. A.; Kokotailo, G. T.; Pasztor, C. T. *J. Am. Chem. Soc.* **1987**, *109*, 7433.

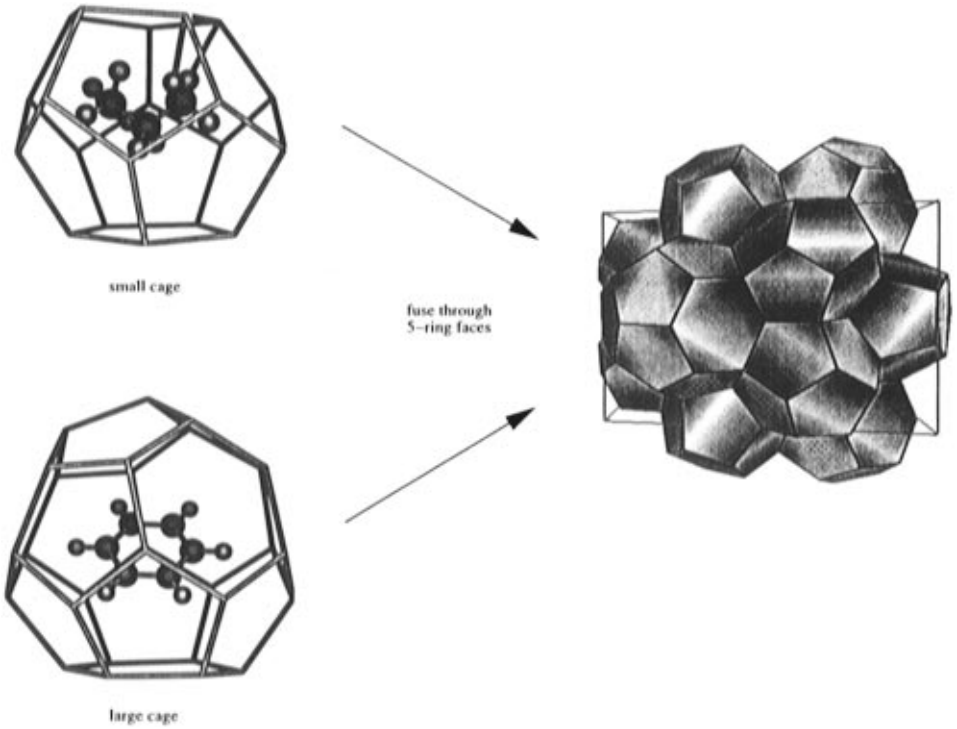

Figure 2. The structure of the clathrasil, dodecasil-3C (MTN), comprised of two types of cage, one a smaller pentagonal dodecahedron and the other a larger hexadecahedron, which are fused through 5-ring windows.

Table 1. Summary of Synthetic Conditions

(a) Variation in Silica Source[a]

silica source	time (days)	products
Cab-O-Sil	5	FER
Ludox LS-30	5	FER
Ludox AS-40	7	FER
silicic acid	5	FER
silica gel	5	FER
sodium silicate	5	amorphous, MTN
tetramethoxysilane	9	FER
α-Quartz	38	α-Quartz

(b) Variation in Reaction Conditions[b]

gel composition					time (days);	
SiO_2	HF/pyr	H_2O	$PrNH_2$	Pyr	temp (°C)	products
1.5	2	8	4	16	5, 170	FER
1.5	2	8	4	16	7, 170	FER
1.5	2	8	4	16	3, 185	FER, minor MTN
1.5	2	8	4	16	5, 185	FER, minor MTN
1.5	2	8	4	16	7, 185	MTN, minor FER
1.5	2	8	4	16	11, 185	MTN
1.5	2	8	4	16	7, 190	MTN
1.5	2	8		16	5, 170	MTN
1.5	2	8	1	19	3, 170	FER
1.5	2	8	4	16	5, 170	FER
1.5	2	8	12	16	5, 170	FER
1.5	2	8	20		5, 170	FER
1.5	2[c]	10	20	0.24	11, 170	MTN
1.5	1	8	4	16	5, 170	FER
1.5	2	8	4	16	5, 170	FER
1.5	4	8	4	16	4, 170	FER
1.5	6	8	4	16	8, 170	FER

[a] Gel composition: 1.5 SiO_2:2 HF/pyridine:8 H_2O:4 $PrNH_2$:16 pyridine. Temperature 170 °C. [b] Silica source: Cab-O-Sil. [c] HF only.

tion, $\lambda = 1.54178$ Å), and studied at room temperature. The cell dimensions were refined by the 2θ values of 25 reflections, $11.2° < 2\theta < 30.2°$. Details of the data collection are given in Table 2. We also collected all possible equivalent reflections for a few Bragg peaks (with $3 < I/\sigma(I) < 11$) to confirm the lowering of symmetry from body centered to primitive. The crystal of dodecasil-3C, obtained from a reaction at 190 °C using both pyridine and propylamine, was also mounted and collected on the CAD-4 diffractometer at room temperature.

3. Magic Angle Spinning (MAS) NMR. ^{29}Si NMR spectra were collected at room temperature on three spectrometers, a Chemagnetics CMX500 and a Bruker AMX500, both operating at 11.7 T, and a Chemagnetics CMX180, operating at 4.2 T. The CMX500 and CMX180 used Chemagnetics double resonance probes (7.5 mm (o.d.) rotors) and the AMX500 used a Doty double resonance probe (5 mm o.d. rotors). Detailed experimental parameters for each spectrum are indicated in the figure captions. Chemical shifts were referenced relative to TMS. Room temperature ^{1}H, ^{29}Si, and ^{13}C MAS NMR spectra were collected on the CMX500 spectrometer for the solid components of the reaction mixture at various time intervals after being heated at 170 °C. In each case the bomb was quenched into water and the solid product obtained by filtration and washing with acetone and/or water. The spectra were all referenced to TMS at 0 ppm.

4. Computer Simulations. Monte Carlo docking calculations were performed to probe the relative stabilities of the templates in each of the zeolite structures using the approach of Freeman and co-workers.[21] The force field derived by Kramer and co-workers[22] was used for the zeolite−zeolite interactions, whereas parameters for interaction of the templates with the zeolite framework were derived from sorption data using standard techniques.[23] Previously fitted molecular mechanics parameters were used to handle interactions within template molecules.[24] Initially, the unloaded zeolite structures were minimized at constant pressure to obtain starting models for the docking calculations. The docking calculations were performed using a fixed zeolite lattice initially, with this constraint being removed for the final stage of the minimization procedure. The DIZZY software was used to perform all the calculations.[25,26] The calculations were performed on a Silicon Graphics Challenge XL machine with 128Mb of memory.

(21) Freeman, C. M.; Catlow, C. R. A.; Thomas, J. M.; Brode, S. *Chem. Phys. Lett.* **1991**, *186*, 136.
(22) Kramer, G. J.; Farragher, N. P.; van Beest, B. W. H.; van Santen, R. A. *Phys. Rev. B* **1991**, 5068.
(23) Henson, N. J.; D. Phil. Thesis, University of Oxford, 1996.
(24) Oie, T.; Maggiora, G. M.; Christoffersen, R. E.; Duchamp, D. D. *Int. J. Quantum Chem., Quantum Biol. Suppl.* **1981**, *1*, 1.
(25) DIZZY software written and developed by N. J. Henson, University of Oxford and University of California, Santa Barbara, 1992−1995.

Table 2. Crystallographic Data for the X-ray Structure Refinement of Templated Ferrierite

formula	$Si_{18}O_{36}$·1.9 C_5H_5N·0.1 C_3H_9N	scan technique	$\Omega/2\theta$
M_r	1237.72	θ, deg	$1 < \theta < 72$
crystal system	orthorhombic	reflcns meas	6841
space group	*Pmnn* (no. 58)	independent reflcns	1975
a, Å	18.8273(6)	obsd reflcns	894
b, Å	14.095(1)	criterion for obsd	$I > 3\sigma(I)$
c, Å	7.4318(7)	scan speed	variable
V, Å^3	1972.2(3)	R_{int}	0.0319
Z	2	refined parameters	170
F(000)	1416	final refinement	anisotropic
temp, °C	25	treatment of hydrogens	refU
D_m, g/cm^3	2.08	*R*	0.0312
μ, cm^{-1}	67.42	R_w	0.0347
crystal shape and color	colorless hexagonal plates	S, goodness of fit	0.916
crystal dimensions, mm	$0.25 \times 0.25 \times 0.01$	average shift/error	0.0061
goniometer	κ-geometry	weighting scheme	3 terms Chebyshev
X-ray source	rotating anode	$(\Delta\varrho)_{min}$ (e Å^{-3})	−0.418
radiation	graphited-monochromated Cu Kα ($\lambda = 1.54178$ Å)	$(\Delta\varrho)_{max}$ (e Å^{-3})	0.418

Results

1. Synthetic Studies. From the trends that are apparent in Table 1, it appears that ferrierite (FER) is obtained under kinetic control in this synthesis and that dodecasil-3C (MTN) is a thermodynamically more stable product. For example, the standard reaction at 170 °C yields FER but the same reaction at 190 °C produces MTN. Furthermore, at intermediate temperatures, e.g. 185 °C, FER forms after 3−5 days, but recrystallizes to yield MTN after 7−11 days. The behavior represents a good illustration of Ostwald's law of successive crystallization.

It is also clear that propylamine plays a central role in the reaction, since the use of a wide range of other amines (e.g. isopropylamine, methylamine, *tert*-butylamine, 2,2-dipyridyl, quinuclidine, collidine) yields alternative products, typically MTN or amorphous silica. Other amines that yield FER are RNH_2 (R = C_4H_9, C_5H_{11}), R_2NH (R = C_3H_7), and 1,3-diaminopropane. We also observe that the use of larger quantities of propylamine reduces the crystallite size. On the other hand, MTN is obtained as the sole product in the absence of propylamine, as reported previously.[19]

The source of silica is also seen to be important. For example, the use of tetramethoxysilane (TMOS) gives only minor quantities of FER after 5 days, apparently because the release of methanol reduces the rate of the zeolite crystallization. On the other hand, the use of α-quartz gives no FER at all, even after 38 days, presumably because it retards the rate of dissolution of the SiO_2. The crystallization rate and crystal size are affected by the HF concentration, with larger crystals being formed at higher concentrations.

2. Crystallographic Findings. The structure of the ferrierite reaction product was refined in space group *Pmnn*, a thorough examination of the diffraction data having revealed a substantial number of reflections that violate the commonly-used body centered space group, *Immm*. Pyridine and propylamine molecules were initially located in both structures by difference Fourier methods. The pyridine hydrogen atoms in calculated positions were held in the "riding" mode with two common isotropic thermal parameters (one for each molecule). Refinement of the FER structure was performed with CRYSTALS[27] and MTN was done using the X-ray 80 package of programs.[28]

Table 3. Final Atomic Coordinates and Equalized Temperature Factors (ESDs in Parentheses) for the Templated Ferrierite Structure

atom	*x*	*y*	*z*	*U*(iso)	Occ
Si(1)	0.15332(6)	0.0000	0.0000	0.0102	1.0000
Si(2)	0.08359(4)	0.20073(6)	0.0132(3)	0.0062	1.0000
Si(3)	0.27289(4)	−0.0010(3)	0.2928(1)	0.0081	1.0000
Si(4)	0.3267(1)	0.1986(2)	0.2128(2)	0.0111	1.0000
Si(5)	0.1778(1)	0.2946(2)	−0.2999(2)	0.0074	1.0000
O(1)	0.0000	0.2118(3)	0.0158(7)	0.0191	1.0000
O(2)	0.2496(2)	0.0000	0.5000	0.0145	1.0000
O(3)	0.1041(1)	0.0912(2)	−0.0218(4)	0.0167	1.0000
O(4)	0.2026(1)	−0.0138(2)	0.1753(3)	0.0167	1.0000
O(5)	0.2457(2)	−0.2396(2)	0.2355(5)	0.0097	1.0000
O(6)	0.3435(1)	−0.2189(2)	−0.0058(6)	0.0165	1.0000
O(7)	0.1187(3)	0.2449(3)	−0.1698(5)	0.0230	1.0000
O(9)	0.1113(2)	0.2565(3)	0.1810(5)	0.0176	1.0000
O(10)	0.3167(2)	0.0851(2)	0.2452(5)	0.0174	1.0000
O(11)	0.3225	−0.0968	0.2541	0.0050	1.0000
N(1)	0.0000	−0.0925(6)	0.4771(2)	0.0554	0.5000
C(1)	0.0000	−0.1127(8)	0.4721(2)	0.1036	0.5000
C(2)	0.0602(4)	−0.0490(5)	0.4879(1)	0.0862	1.0000
C(3)	0.0000	−0.4386(6)	0.3508(8)	0.0879	0.92(1)
C(4)	0.0000	−0.4074(5)	0.5588(8)	0.0642	0.92(1)
C(5)	0.0000	−0.4745(7)	0.6909(7)	0.1154	0.92(1)
C(100)	0.0000	−0.4505(8)	0.4722(6)	0.0277(4)	0.09(1)
C(200)	0.0000	−0.3898(8)	0.6337(9)	0.0361(4)	0.09(1)
H(1)	0.0000	−0.1868(8)	0.4568(2)	0.1005(4)	0.5000
H(2)	0.1084(4)	−0.0864(5)	0.4802(1)	0.1005(4)	1.0000
H(3)	0.0000	−0.3859(6)	0.2511(8)	0.0483(4)	0.6700
H(4)	0.0000	−0.3352(5)	0.5943(8)	0.0483(4)	0.6700
H(5)	0.0000	−0.4549(7)	0.8272(7)	0.0483(4)	0.6700

Final atomic coordinates and temperature factors are given in Table 3, and selected bond distances and angles are presented in Table 4.

The crystal structure of the ferrierite is shown in Figures 3 and 4. The silica framework is quite similar to that of a sample from which the guest molecules have been removed by calcination,[15] although the Si(1) tetrahedron appears to be subject to some angular distortion due to the proximity of the pyridine guest molecules. Other, more subtle changes are also observed, such as the 1.7° increase in the average Si−O−Si angle; this appears to stem largely from the expansion of the cell in the presence of the template (for siliceous ferrierite,[15] $a = 18.720(1)$ Å; $b = 14.070(1)$ Å; $c = 7.4197(1)$ Å; $V = 1954.3$ Å^3). The SiO_4 tetrahedra are quite regular compared with aluminosilicate zeolites, primarily due to the absence of effects due to exchangeable cations. However, the units do show an appar-

(26) Auerbach, S. M.; Henson, N. H.; Cheetham, A. K.; Metiu, H. I. *J. Phys. Chem.* **1995**, *99*, 10600.

(27) Watkin, D. J.; Carruthers, J. R.; Betteridge, P. W. *CRYSTALS user guide*; Chemical Crystallography Laboratory: Oxford, 1990.

(28) Stewart, J. M.; Kundel, F. A.; Baldwin, J. C. *The X-ray system*; (Computer Science Center) University of Maryland; 1980.

(29) Hriljac, J. A.; Eddy, M. M.; Cheetham, A. K.; Donahue, J. A.; Ray, G. J. *J. Solid State Chem.* **1993**, *106*, 66.

Table 4. Bond Distances (Å) and Bond Angles (deg) with ESDs for the Templated Ferrierite Structure

Si(1)−O(3)	1.593(2)	Si(5)−O(7)	1.632(5)
Si(1)−O(3)	1.593(2)	Si(5)−O(10)	1.731(4)
Si(1)−O(4)	1.611(2)	N(1)−C(2)	1.291(8)
Si(1)−O(4)	1.611(2)	N(1)−C(2)	1.291(8)
Si(2)−O(1)	1.5817(9)	C(1)−C(2)	1.45(1)
Si(2)−O(3)	1.612(2)	C(1)−C(2)	1.45(1)
Si(2)−O(7)	1.635(4)	C(2)−C(2)	1.39(1)
Si(2)−O(9)	1.564(4)	C(3)−C(4)	1.608(8)
Si(3)−O(2)	1.601(1)	C(3)−C(5)	1.26(1)
Si(3)−O(4)	1.596(3)	C(3)−C(100)	0.918(7)
Si(3)−O(10)	1.510(4)	C(4)−C(5)	1.363(9)
Si(3)−O(11)	1.667(4)	C(4)−C(100)	0.89(1)
Si(4)−O(5)	1.638(5)	C(4)−C(200)	0.61(1)
Si(4)−O(6)	1.680(6)	C(5)−C(100)	1.660(8)
Si(4)−O(9)	1.545(5)	C(5)−C(100)	1.61(1)
Si(4)−O(11)	1.469(3)	C(5)−C(200)	1.27(1)
Si(5)−O(5)	1.570(5)	C(100)−C(100)	1.45(2)
Si(5)−O(6)	1.511(6)	C(100)−C(200)	1.47(1)
O(3)−Si(1)−O(3)	108.9(2)	O(2)−Si(3)−O(11)	109.1(2)
O(3)−Si(1)−O(4)	120.9(1)	O(4)−Si(3)−O(11)	106.2(2)
O(3)−Si(1)−O(4)	98.9(1)	O(10)−Si(3)−O(11)	107.7(1)
O(3)−Si(1)−O(4)	98.9(1)	O(5)−Si(4)−O(6)	102.4(2)
O(3)−Si(1)−O(4)	120.9(1)	O(5)−Si(4)−O(9)	120.4(2)
O(4)−Si(1)−O(4)	109.7(2)	O(6)−Si(4)−O(9)	106.4(2)
O(1)−Si(2)−O(3)	109.6(2)	O(5)−Si(4)−O(11)	105.9(2)
O(1)−Si(2)−O(7)	112.0(3)	O(6)−Si(4)−O(11)	112.2(2)
O(3)−Si(2)−O(7)	97.7(2)	O(9)−Si(4)−O(11)	109.5(2)
O(1)−Si(2)−O(9)	105.8(2)	O(5)−Si(5)−O(6)	116.4(2)
O(3)−Si(2)−O(9)	122.0(2)	O(5)−Si(5)−O(7)	99.4(2)
O(7)−Si(2)−O(9)	109.7(1)	O(6)−Si(5)−O(7)	109.4(2)
O(2)−Si(3)−O(4)	107.5(2)	O(5)−Si(5)−O(10)	112.1(2)
O(2)−Si(3)−O(10)	111.6(3)	O(6)−Si(5)−O(10)	108.9(2)
O(4)−Si(3)−O(10)	114.6(2)	O(7)−Si(5)−O(10)	110.2(2)
Si(2)−O(1)−Si(2)	168.6(3)	Si(4)−O(6)−Si(5)	148.6(2)
Si(3)−O(2)−Si(3)	148.2(2)	Si(2)−O(7)−Si(5)	158.7(3)
Si(1)−O(3)−Si(2)	153.6(2)	Si(2)−O(9)−Si(4)	149.9(3)
Si(1)−O(4)−Si(3)	155.0(2)	Si(3)−O(10)−Si(5)	149.9(3)
Si(4)−O(5)−Si(5)	164.4(3)	Si(3)−O(11)−Si(4)	149.0(1)

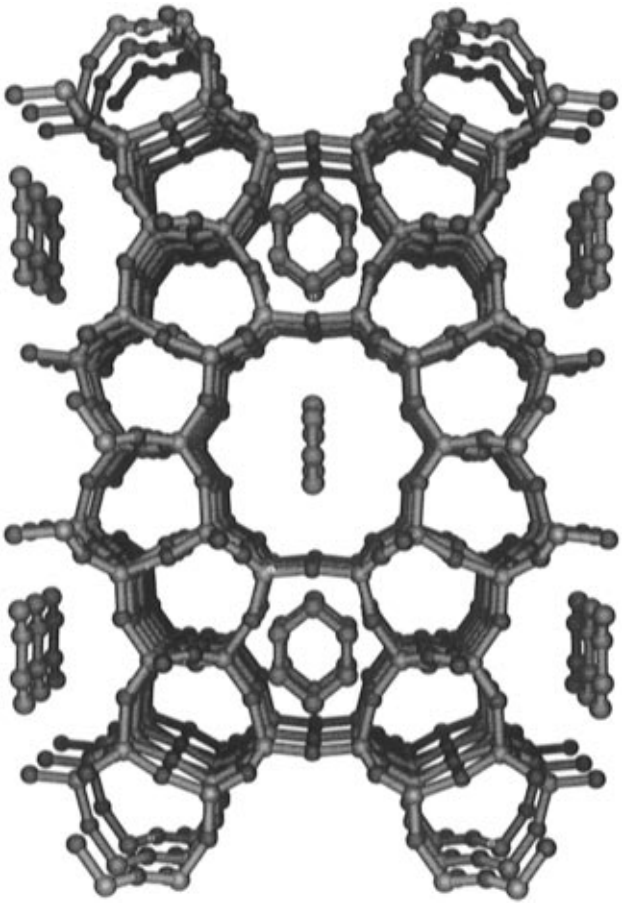

Figure 3. The structure of templated FER viewed down the [001] direction showing the pyridine and propylamine molecules (not superimposed for clarity) in the 10-ring channel and the pyridine molecules lying parallel to the [010] direction in the 8-ring channel; hydrogen atoms are not shown.

ently larger range of bond lengths (1.469−1.731 Å) than is found in, say, siliceous Y (1.597−1.614 Å),[29] probably as a consequence of the diminished precision that arises from the pseudo-body-centered nature of the structure. The Si−O−Si bond angles range from 148.2° to 168.6°, the latter corresponding to the angle that is required to be linear in the *Immm* description of the structure.[14]

The first pyridine molecule is located in the side channel, in a cavity that is delineated by the 8-ring and 6-ring windows (Figure 3). A careful examination of the distances and thermal factors enables us to determine the location of the nitrogen of the pyridine molecule. Because of its position relative to the mirror plane, the pyridine has two orientations, opposite to each other. This implies that both N(1) and C(1) have an occupancy of 0.5. In addition, the van der Waals contacts with the framework appear to be optimized; the shortest distance to the framework (C/N···O) is 3.58 Å. Aside from the interaction with the Si(1) tetrahedron (see above), the pyridine-framework interactions lead to some small changes in Si−O−Si angles which are also apparent in the ^{29}Si MAS NMR spectrum (see below). The pyridine is essentially trapped in the side channel cavity, as a consequence of which it is quite difficult to remove; calcination in dry oxygen for 48 h at 800 °C is required to remove all traces of pyridine.[15] The high-temperature weight loss in the TGA measurements (6.1 wt %) is in reasonable agreement with the expected change due to the loss of pyridine in this temperature range (6.8 wt %).

In contrast to the chemical composition reported in a previous synthesis of ferrierite[30] using the same procedure, we find no evidence for HF in the product by chemical analysis or vibrational spectroscopy. A second pyridine molecule is found in the main 10-ring channel of the structure, together with a small amount of propylamine. Refinement of the occupancy for each molecule, considered as independent parameters, converged to 90% for pyridine and 12% for propylamine. Since both molecules cannot be located in the same place at the same time, the sum of their occupancy was restrained to 1.00(1), giving final occupancies of 0.92(1) and 0.09(1) for the pyridine and the propylamine, respectively. The positions of the nitrogen atoms could not be determined, either for the pyridine or the propylamine. The relative orientations of both pyridine molecules are shown in Figure 4. To maximize its van der Waals contacts with the oxygen atoms of the framework [closest (C/N···O) distance being 3.48 Å for pyridine and 3.13 Å for propylamine], the pyridine molecules tilt when compared to the framework topology, as discussed below.

In the case of the crystal structure of dodecasil-3C (MTN), we have confirmed the tetragonal structure in *I*42*d* observed by Chae *et al.*[19] (a = 13.639(2) Å, c = 19.512(4) Å, R = 0.068 for 736 reflections with $I > 3\sigma(I)$). Approximately 80% of the larger cages contain pyridine, and we also find ∼25% occupancy of the smaller cages by propylamine (the previous work was based upon a synthesis involving pyridine but no propylamine).

3. MAS NMR Studies. The ^{29}Si NMR spectrum of the templated ferrierite product is compared in Figure 5 with the

(30) Nadimi, S.; Oliver, S.; Kuperman, A.; Lough, A.; Ozin, G. A.; Garces, J. M.; Olken, M. M.; Rudolf, P. *Studies in Surface Science and Catalysis*; 1994; Vol. 84A, p 93.

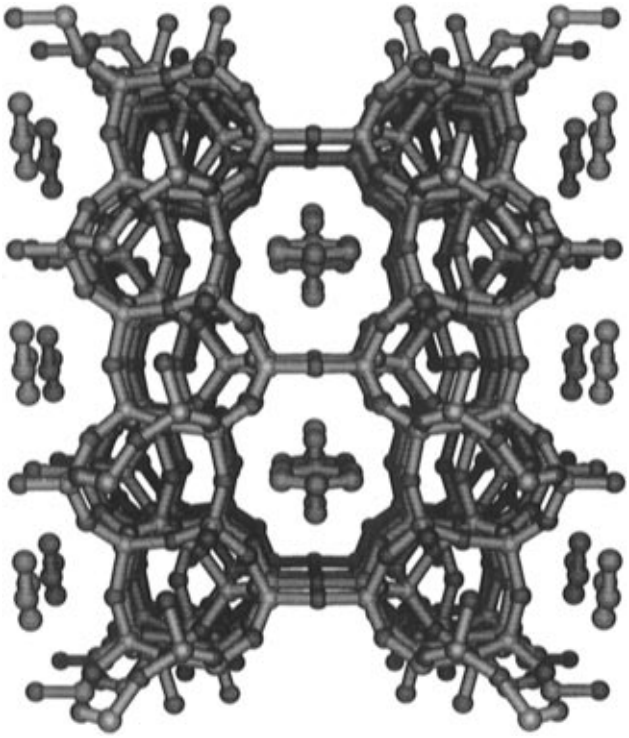

Figure 4. The structure of templated FER viewed down the [010] direction showing the two orientations of the pyridine molecules; hydrogen atoms are not shown.

corresponding spectrum of a sample from which the template has been removed by calcination. After calcination, it is apparent that most of the lines have shifted downfield. It has been shown that the ^{29}Si chemical shifts in well-characterized siliceous zeolites correlate well with a simple function ($\cos\alpha/(\cos\alpha - 1)$) of the Si−O−Si bond angles, α, around each Si site.[31,32] Our ^{29}Si NMR results are in agreement with these correlations; the chemical shifts move to higher fields in the templated form, where the average of the Si−O−Si bond angles around each Si site is found to be larger than those in the calcined FER.

The ^{29}Si MAS NMR spectra and the corresponding X-ray patterns of samples taken from the FER reaction as a function of time at 170 °C, and then washed with acetone, are shown in Figure 6. During the early stages of the reaction, the ^{29}Si spectra reveal not only the broad feature due to the silica gel, but also an unexpected crystalline intermediate with a chemical shift that is consistent with the presence of octahedrally coordinated silicon. The ^{29}Si and the additional ^{1}H and ^{13}C NMR spectra (not shown here) lead us to believe that it is a propylammonium hexafluorosilicate salt that forms at the onset of the reaction. A preliminary indexing of the powder X-ray pattern points to a monoclinic phase with $a = 5.106$ Å, $b = 6.774$ Å, $c = 11.530$ Å, $\beta = 98.50°$. This phase dissolves rapidly when the reaction product is washed in water, whereas it is found to be insoluble in acetone.

The ^{13}C MAS NMR spectra of the template-containing FER, washed with water and with acetone, are compared in Figure 7. The water-treated sample contains both pyridine and propylamine in a ratio of 20:1, in good agreement with the crystallography. The spectra of the acetone-washed samples are dominated by signals from pyridine in the FER and the propylammonium cation in the hexafluorosilicate salt.

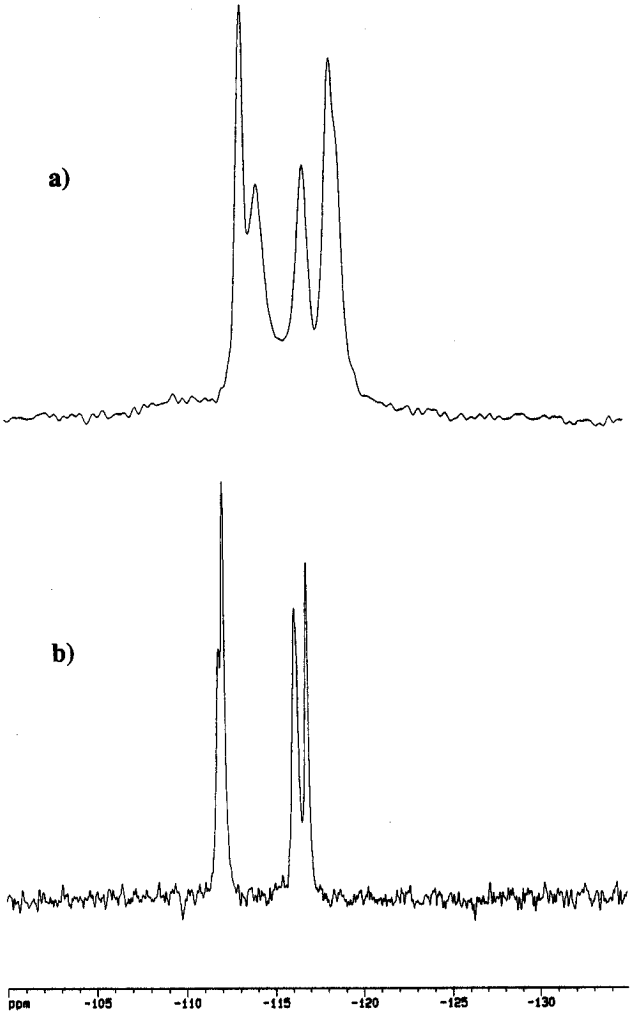

Figure 5. The ^{29}Si magic angle spinning NMR spectra of (a) the templated ferrierite product and (b) of the corresponding calcined sample. The spectra were collected with proton decoupling during acquisition and a recycle delay of 5 min. Rotor spinning speeds of ~6 kHz were used.

4. Computational Studies. Previous lattice energy calculations by us have indicated[15] that the energies of ferrierite (+11.3 kJ mol^{-1}) and dodecasil-3C (+10.8 kJ mol^{-1}) per SiO_2 unit, relative to α-quartz, *in the absence of template molecules*, are almost identical. It has been shown, both experimentally[33] and computationally,[34] that the heats of formation of the silica polymorphs span a range of only ~15 kJ mol^{-1} between α-quartz and the open framework of siliceous faujasite, and it has been shown that the energy is dependent on framework density.[35,36] This is consistent with the small difference in the calculated lattice energies for ferrierite and dodecasil-3C, since their densities differ only by 0.05 g cm^{-3}.

The docking calculations performed here probe the relative binding energetics of the template molecules in the zeolite frameworks. The results are shown in Table 5. The predicted orientations of the pyridine molecules in ferrierite reproduce the crystallographic positions quite closely, clearly showing the tilting of the molecules with respect to the framework (Figure

(31) Fyfe, C. A.; Feng, Y.; Grondy, H. *Microporous Mater*. **1993**, *1*, 393.
(32) Dupree, R.; Cohn, S. C.; Henderson, C. M. B.; Bell, A. M. T. In *Nuclear Magnetic Shielding & Molecular Structure*; NATO ASI; Tossell, J. A., Ed.; 1992; Vol. 386, p 421.
(33) Petrovic, I.; Navrotsky, A.; Davis, M. E.; Zones, S. I. *Chem. Mater*. **1993**, *5*, 1805.
(34) Henson, N. J.; Cheetham, A. K.; Gale, J. D. *Chem. Mater*. **1994**, *6*, 1447.
(35) de Vos Burchart, E.; Verheij, V. A.; van Bekkum, H.; van de Graaf, B. *Zeolites* **1992**, *12*, 183.
(36) Kramer, G. J.; de Man, A. J. M.; van Santen, R. A. *J. Am. Chem. Soc*. **1991**, *113*, 6435.

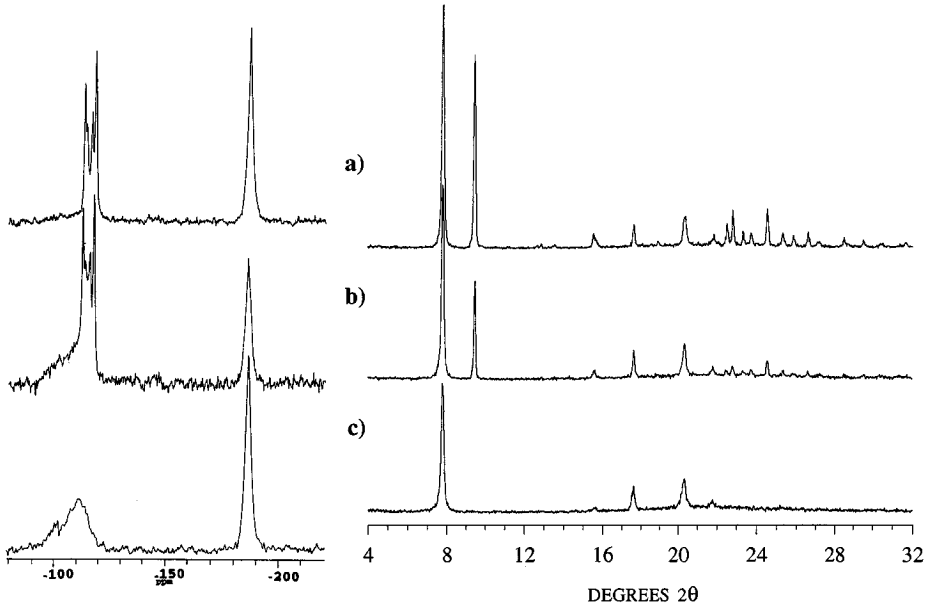

Figure 6. The ^{29}Si magic angle spinning NMR spectra and the corresponding X-ray patterns of samples taken from the FER reaction after being heated at 170 °C and then washed with acetone. Reaction times were (a) 20 h, (b) 6 h, and (c) 2 h.

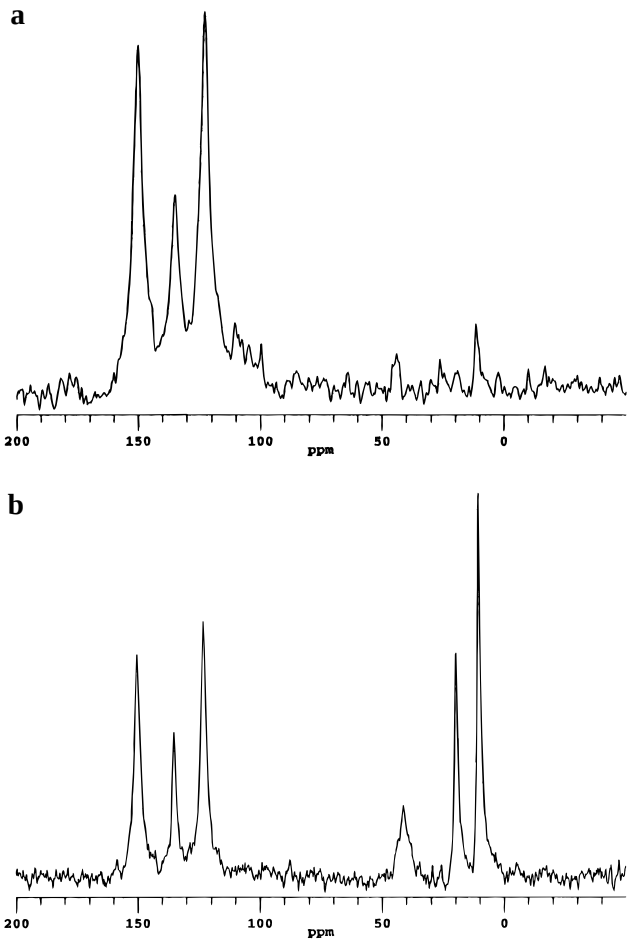

Figure 7. The ^{13}C magic angle spinning NMR spectra of the template-containing FER, washed with (a) water and (b) acetone. The spectra were collected with proton decoupling during acquisition of the signal. The recycle time for both spectra was 20 s, and the rotor spinning speeds were ∼5 kHz. Peaks at 150.8, 135.7, and 123.5 ppm are assigned to pyridine, peaks at 41.9, 20.3, and 10.9 ppm are assigned to propylammonium, and peaks at 44.4, 26.8, and 12.1 ppm are assigned to propylamine.

8), but there are noticeable differences in the propylamine positions (not shown). However, only a small amount of propylamine is located in the crystallographic study and the calculations are revealing several sites that cannot be refined separately. In the case of dodecasil, we predict that the pyridine molecule is too large to occupy the small cage, and is therefore only located in the large cage, causing the propylamine to be found exclusively in the small cage.

Table 5. Calculated Binding Energies for Docked Template Molecules in Ferrierite and Dodecasil-3C (kJ/mol^{-1})

	FER		MTN	
molecule	8-ring channel	10-ring channel	small cage	large cage
pyridine	78	62	no site	76
propylamine	79	70	78	73

Discussion

The results presented in Table 1 demonstrate clearly that the synthesis of ferrierite is critically dependent upon a number of parameters, but several observations from the synthetic work shed light on the mechanism of its crystallization and the subtle interplay between the kinetic and thermodynamic factors that favor the formation of FER and MTN, respectively. For example, since the use of propylamine at 170 °C results in the synthesis of FER, but the absence of the amine (or the use of alternative amines) leads to the formation of MTN, it is clear that propylamine is involved in a crucial step in the kinetic process that leads to the initial crystallization of ferrierite. The presence of propylamine during the FER synthesis will clearly reduce the acidity of the solution, since it is present in a 2-fold molar excess over the HF and forms the propylammonium salt of SiF_6^{2-}. It will also ensure that the pyridine is unable to form substantial amounts of the pyridinium cation. On the other hand, the propylamine cannot act merely as a proton sponge, since other primary amines, such as methylamine, do not facilitate the formation of FER. We propose that small silicate precursors of the ferrierite structure are nucleated by propylammonium cations, an observation that is consistent with the detection of small quantities of propylamine in the final product and with the decrease in crystal size when larger quantities of the base are used. Closely related amines (e.g. RNH_2 ($R = C_4H_9$, C_5H_{11}), R_2NH ($R = C_3H_7$), and 1,3-diaminopropane) are also able to

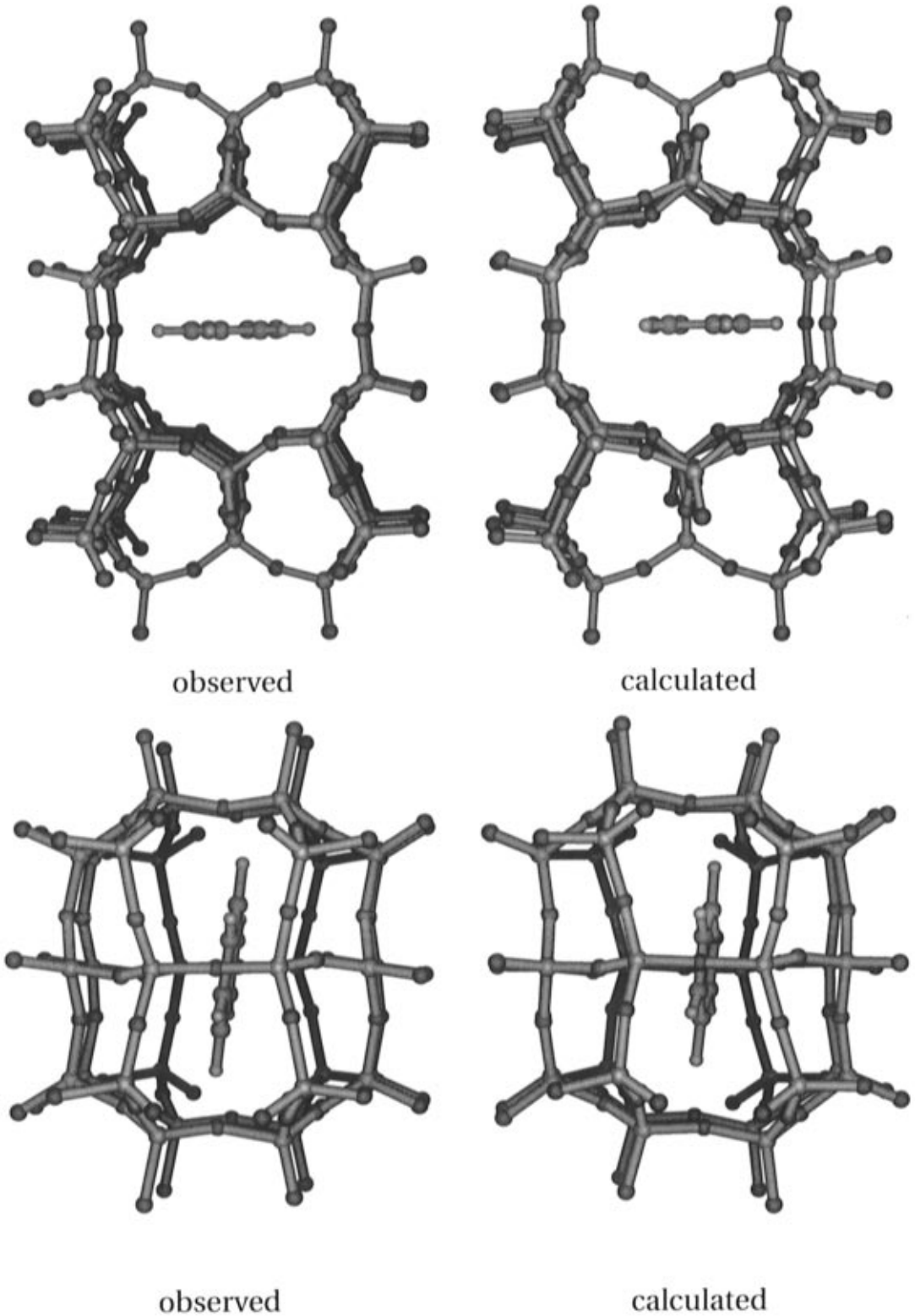

Figure 8. Comparison of the single-crystal X-ray diffraction (obs) and computer simulations (calc) showing (a, top) the pyridine molecule in the main channel down [001] and (b, bottom) the pyridine molecule in the side channel viewed down [100].

perform this function. The low concentration of propylamine found in the FER product indicates that the primary amine is not an important factor in the thermodynamic stability of the ferrierite, though it will contribute more to the MTN where it occupies the small cage to a level of ~25%.

The role of pyridine in the competitive formation of FER and MTN is apparently quite different. Since it is present in both products in substantial quantities, it has a significant influence on the stabilities of the two phases. Pyridine clearly participates in the growth of the ferrierite crystals, into which it is incorporated in almost stoichiometric amounts into both the 10-ring channel and the side channel. The complete pore filling of the framework by pyridine may be related to why ferrierite is the first phase to form. Since the hexagonal plate-like crystals have a short dimension along the [100] direction, it seems likely that the crystal growth takes place along [010] and [001]. Our results are consistent with a model in which the pyridine is laid down, layer by layer, in partial cavities or pockets, as illustrated in Figure 9; the cavities are then completed by the deposition of a further layer of silicate and pyridine. This

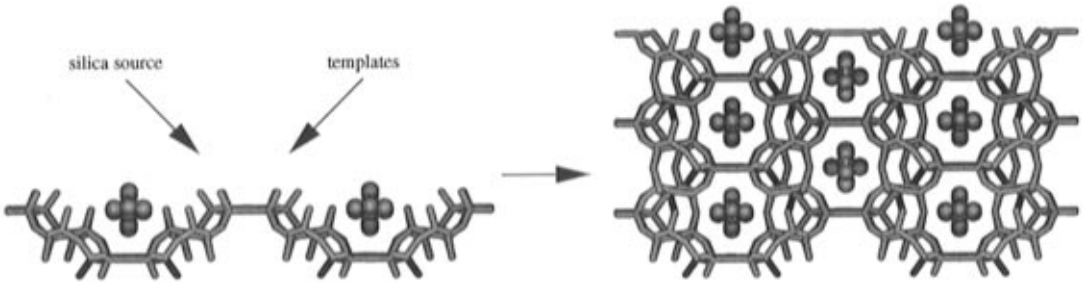

Figure 9. A schematic showing a possible mechanism for the crystal growth of FER. Pyridine is laid down, layer by layer, in partial cavities or pockets. The cavities are then completed by the deposition of a further layer of silicate and pyridine.

mechanism, which is compatible with the strong binding of pyridine in the cavities (Table 5), has been proposed in the case of the synthesis of EMT in the presence of crown ethers[3] and is consistent with the incorporation of tetrapropylammonium cations into ZSM-5 at an early stage during crystal growth.[5]

It is interesting to consider the role of water in the synthesis of FER and MTN. Although increasing the amount of water does not significantly change the reaction kinetics, and we find no evidence for water in either crystal structure, it is nevertheless an essential component since the reaction will not proceed without it. Small amounts of water present in the gel probably aid in the hydrolysis of SiF_6^{2-}, resulting in the formation of silicate species and HF. The water also probably acts as the mass transfer medium when FER transforms into MTN.

Our findings have enabled us to explore some of the complex factors that can influence crystallization processes during zeolite synthesis. The mechanism that is evolving from the present work involves classical nucleation and growth stages in which different organic species play key roles. The initial nucleation of the FER structure appears to be driven by the presence of propylammonium cations; pyridine is then incorporated into the channels of the structure in almost stoichiometric amounts during the growth of the zeolite crystallites. In the absence of propylamine, some of the pyridine will be protonated and MTN is found to be the sole product, leading us to suggest that pyridinium is the nucleating species in this instance. Both pyridine and propylamine are incorporated into the MTN crystals during the growth phase. The formation of MTN during longer reactions at lower temperatures may also stem from slow nucleation of the former structure in the presence of very small concentrations of pyridinium cations. The crystallization of the more stable MTN is facilitated by the use of higher temperatures. The energies of the parent FER and MTN frameworks are almost identical and the calculated binding energies of both organic molecules are very similar (Table 5). However, since the loading of sorbates is approximately twice as high in FER, it seems likely that the FER product has a slightly more favorable enthalpy. Entropic factors associated with the loss of adsorbed species must therefore drive the transformation of FER into MTN.

Acknowledgment. The work was funded by the MRL program of the National Science Foundation under award DMR 9123048. N.J.H. thanks the SERC (UK) for a studentship and J.C.G. thanks the French Foreign Affairs Ministry for a "Lavoisier" fellowship. Figures 1, 2, 3, 4, 8, and 9 were generated using the Insight II and Catalysis Software Suite written and developed by Biosym Technologies.

Supporting Information Available: Tables of Bragg peaks measured at very low scan speed that violate the body-centered extinction rules (3 pages). This material is contained in many libraries on microfiche, immediately follows this article in the microfilm version of the journal, can be ordered from the ACS, and can be downloaded from the Internet; see any current masthead page for ordering information and Internet access instructions.

JA952418G